ADVANCED FUNCTIONAL MATERIALS
www.afm-journal.de

Spontaneous Formation of Liquid Crystals in Ultralarge Graphene Oxide Dispersions

*Seyed Hamed Aboutalebi, Mohsen Moazzami Gudarzi, Qing Bin Zheng, and Jang-Kyo Kim**

A novel process is developed to synthesize graphene oxide sheets with an ultralarge size based on a solution-phase method involving pre-exfoliation of graphite flakes. Spontaneous formation of lyotropic nematic liquid crystals is identified upon the addition of the ultralarge graphene oxide sheets in water above a critical concentration of about 0.1 wt%. It is the lowest filler content ever reported for the formation of liquid crystals from any colloid, arising mainly from the ultrahigh aspect ratio of the graphene oxide sheets of over 30 000. It is proposed that the self-assembled brick-like graphene oxide nanostructure can be applied in many areas, such as energy-storage devices and nanocomposites with a high degree of orientation.

1. Introduction

Graphene is an intriguing and interesting new class of carbon-based nanoscale material with many unusual and fascinating properties that are distinct from those of other graphitic systems.[1] Since the first attempt to obtain monolayer graphene sheets by mechanical exfoliation of graphite,[2] many potential applications of graphene have been introduced to put its fascinating properties into practice. However, widespread use of its properties requires the development of cost-effective routes to achieve full exfoliation of graphite and mass production of graphene sheets with high quality.[3] Among the many methods that have been studied, the chemical reduction of graphite oxide – a layered material assumed to consist of hydrophilic graphene sheets containing oxygen functional groups in the form of carboxyl, hydroxyl or epoxy groups on their basal planes and edges[4,5] – is considered to be the most facile to fabricate covalently functionalized single-layer graphene oxide (GO).[6] The presence of oxygen functional groups provides the advantage of introducing multifunctionalities[5] allowing high solubility of GO in water and other polar solvents.[7] Currently, the solution-based chemical method possesses unrivalled advantages in terms of yield and cost over other methods such as micromechanical exfoliation,[2] chemical-vapor deposition[8] and epitaxial growth,[9] all of which produce an extremely low yield and cannot be used in large-scale applications of graphene.

A common approach to the synthesis of exfoliated graphite using the chemical method is the use of concentrated acids in the presence of a strong oxidizing agent to yield graphite oxide.[10–13] This process is accompanied by an increase in the *d*-spacing between the graphene layers from about 0.34 to ≈0.6–1.2 nm,[14] which is directly related to the degree of oxidation and the hydration level. The large interlayer distance allows water molecules to be effectively intercalated,[13] resulting in easy dispersion of GO in aqueous media.

Chemical methods have been widely used to produce GO whose lateral size is often very small, namely in the range of hundreds of nanometers to a few micrometers at best. The reason behind the small GO size lies in the way that these GO sheets are prepared. In almost all synthesis processes, intercalation and dispersion are achieved via ultrasonication, inevitably resulting in severe breakage of graphene sheets into small pieces.[15,16] The diameter, or lateral size, is often too small to use for the fabrication of electronic devices using microelectronics processes.[17] Provided that large-size graphene sheets can be produced, there are numerous advantages to be realized in the areas of electronics,[18] molecular sensors,[19] and composite materials.[17] For instance, large-size GO sheets with 20% of them being larger than 25 μm in diameter have been fabricated[18] where the electrical properties were much better than for smaller ones because of the much-lower degree of defects on their basal planes, arising from the lower degree of non-stoichiometric oxygen. Fabrication of large GO sheets, with around 50% of them being larger than 10 μm in diameter, has also been reported.[20] There is a similar report regarding liquid dispersions of graphene in an inorganic solvent, *N*-methylpyrrolidone (NMP), using a potassium-intercalated graphite compound without sonication.[21] Liquid-phase dispersions in organic solvents typically yield solutions with low graphene concentrations, say 0.15 mg mL^{-1}.

In addition to the superior electrical conductivities, GO sheets with a large lateral size in colloidal suspensions can induce a transition from the isotropic to a liquid-crystalline structure, which is directly related to the aspect ratio of the filler particles and the viscosity of the solvent.[20] The liquid-crystalline structure is of potential technological interest[22] because the self-aligned GO sheets produced by the liquid-crystalline process can give rise to much-enhanced physical and mechanical properties. Liquid-crystalline materials in the form of lyotropic

---

S. H. Aboutalebi, M. M. Gudarzi, Q. B. Zheng, Prof. J.-K. Kim
Department of Mechanical Engineering
Hong Kong University of Science and Technology
Clear Water Bay, Kowloon, Hong Kong, P. R. China
E-mail: mejkkim@ust.hk

DOI: 10.1002/adfm.201100448

nematic phases have been produced previously using different carbon allotropes, ranging from multiwalled carbon nanotubes (CNTs)[23,24] and single-walled CNTs[25–27] to graphene.[28] Driven by a gain in excluded-volume entropy, these liquid-crystal phases may be formed in concentrated suspensions of hard-body rods or plate-like particles.[22,29] Compared to other approaches developed to align GO sheets, the liquid-crystal route is particularly attractive to achieve self-aligned assemblies with high volume fractions of graphitic materials in the form of fibers and films.[24,28,30] A high polydispersity is required to assure a nematic liquid-crystalline phase behavior, according to a simulation.[21] However, the nematic phase is the only probable phase for polydisperse, unfunctionalized systems.[28]

This paper reports a chemical method that involves pre-exfoliation of natural graphite flakes to produce gram quantities of ultralarge (UL), single-layer GO sheets, up to 10 000 μm^2 in area, with a yield exceeding 80%. We demonstrate that high-concentration dispersions of fully soluble material yield lyotropic, nematic, liquid-crystalline aqueous suspensions due to the reorganization of the GO sheets in the liquid.

2. Characteristics and Liquid Crystallinity of GO

2.1. Characteristics of the UL-GO Sheets

Exfoliation of graphite into monolayer GO sheets as a result of the oxidation and washing processes was performed in the absence of a sonication step, resulting in a stable, brown suspension. The suspension exhibited clear anisotropic textures even after gentle shaking, which is typical of GO sheets with large sizes and high aspect ratios.[3] Fabrication of UL-GO sheets depends on two factors: i) the use of large starting graphite flakes and ii) avoiding strong reactions due to vigorous ultrasonication. However, the use of large graphite flakes as the starting material does not necessarily guarantee large-size GO sheets. Therefore, the pre-exfoliation process and the use of exfoliated graphite, instead of using conventional graphite-intercalation compounds, are necessary to avoid the damaging ultrasonication process and thus ensure minimum breakage of the GO sheets during fabrication.

Optical microscopy (OM) was employed to investigate the morphology of the GO sheets. The size and transparency of individual GO sheets consisting of single-atom-thick layers make them very difficult to be visualized under optical microscopy.[31] Atomic force microscopy (AFM) and scanning electron microscopy (SEM) are potentially destructive and are considered inadequate.[32] Typical graphene has an opacity in the order of 2.3 ± 0.1% and negligible reflectance (<0.1%), whereas optical spectroscopy shows that the opacity is practically independent of wavelength, λ, in the visible range. The opacity has been found to increase on increasing the thickness, so that each graphene layer adds another 2.3%.[33] Although there are reports regarding the observation of suspended graphene sheets under bright-field transmitted light, routine identification of graphene sheets is not trivial, especially when they are deposited on a strongly absorbing substrate. GO is generally much paler, with weaker absorbance, than graphene, making direct optical identification of GO much-more difficult than graphene sheets. However, GO sheets are typically exfoliated into single sheets, unlike graphene sheets.

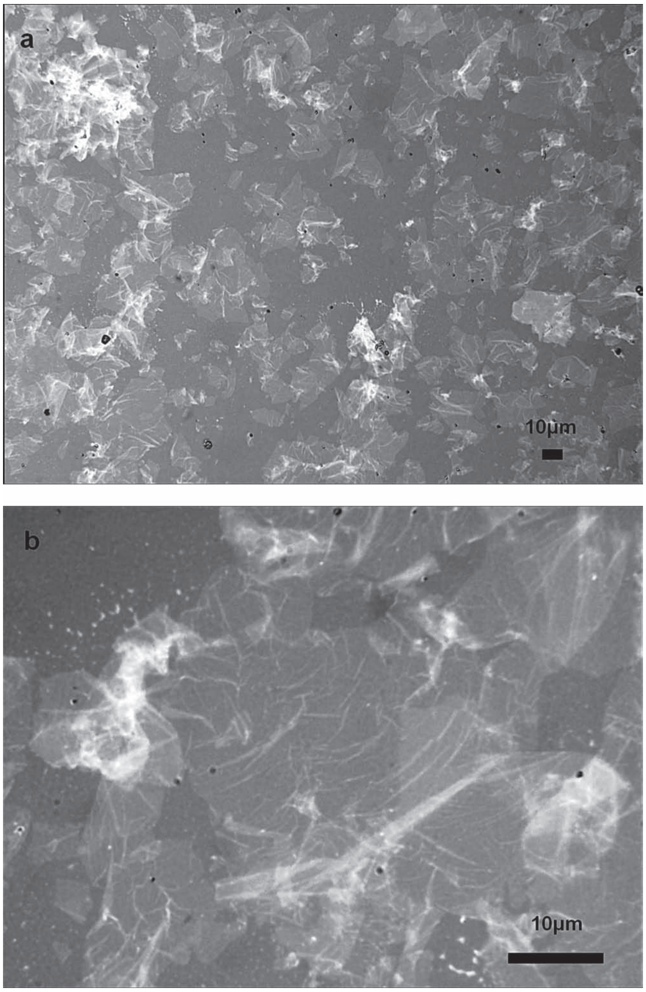

Figure 1. Optical micrographs of as-produced UL-GO sheets at low (a) and high (b) magnifications.

Figure 1 presents typical optical micrographs of the large-size GO sheets produced in this study, confirming a lateral size of tens of micrometers. The corresponding SEM micrograph that can complement the optical microscopy is presented in **Figure 2**, along with the size distribution of the GO sheets. The GO sheets, shown in black, had a lateral size predominantly on the order of 30–50 μm, with many of them being even larger than 70 μm and up to 100 μm. However, fragments of smaller GO sheets, typically 5–10 μm in diameter, were also observed, which are thought to be inevitable due to breakages during the exfoliation process.

The monolayer exfoliation of GO sheets can be further confirmed using transmission electron microscopy (TEM) or AFM. The high-resolution TEM (HR-TEM) images presented in **Figure 3** indicate that the GO sheets indeed consisted of single layers whose size was in excess of several micrometers, in good agreement with the OM observations. Figure 3b shows a torn GO sheet, probably created as a consequence of local high temperature induced by the strong electron beam of the TEM,

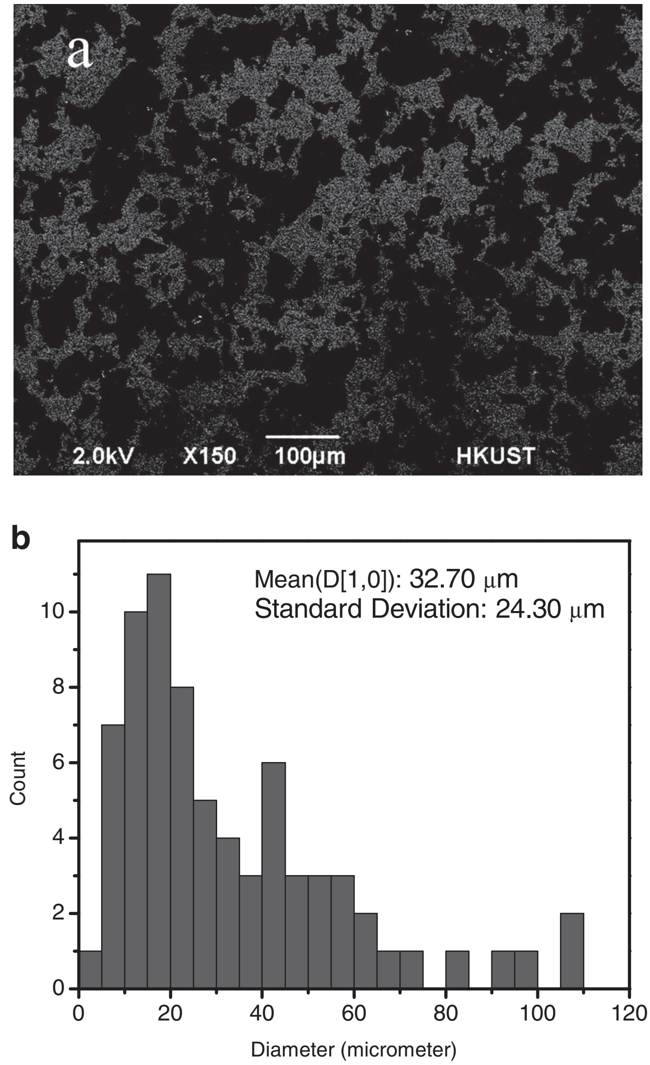

Figure 2. a) SEM micrograph of as-prepared GO sheets. b) Size distribution of as-prepared GO sheets.

thus damaging the GO sheet, as they are known to be sensitive to light and heat. The number of edge-observed in TEM has been used to indicate the number of layers in multilayer GO sheets.[15] The one edge-line clearly noted in Figure 3b confirmed a monolayer GO sheet. The non-crystalline, amorphous carbon structure also suggests a highly oxygenated nature of the GO.

Figure 4 shows a typical AFM image of a GO sheet with wrinkles. By line-scanning across the plain area of the sheet, the height was estimated to be ≈1.06 nm. Because of the existing space between the sheets and substrate due to the evaporation of solvent, the height of ≈1.0 nm estimated here can be viewed as the single graphene sheet, according to previous studies on statistical evaluation.[8,15] The wrinkles observed on the surface are a fundamental morphology found in solution-processed GO or reduced GO structures. The larger the GO size and the more the functional groups attached onto the GO plane, the more likely it is that wrinkling takes place.[34] The GO sheets are expected to be around 1 nm thick due to the presence of covalently bonded oxygen and the displacement of the sp^3-hybridized carbon atoms above and below the original graphene basal plane.[35] The thickness of the GO sheets obtained in this study was in good agreement with results reported in the literature,[20] confirming monolayer GO sheets. The height profiles measured at different locations proved the uniform thickness of the resulting GO sheets.

The structure of the GO sheets was characterized using X-ray-diffraction (XRD) spectroscopy. **Figure 5** shows the XRD

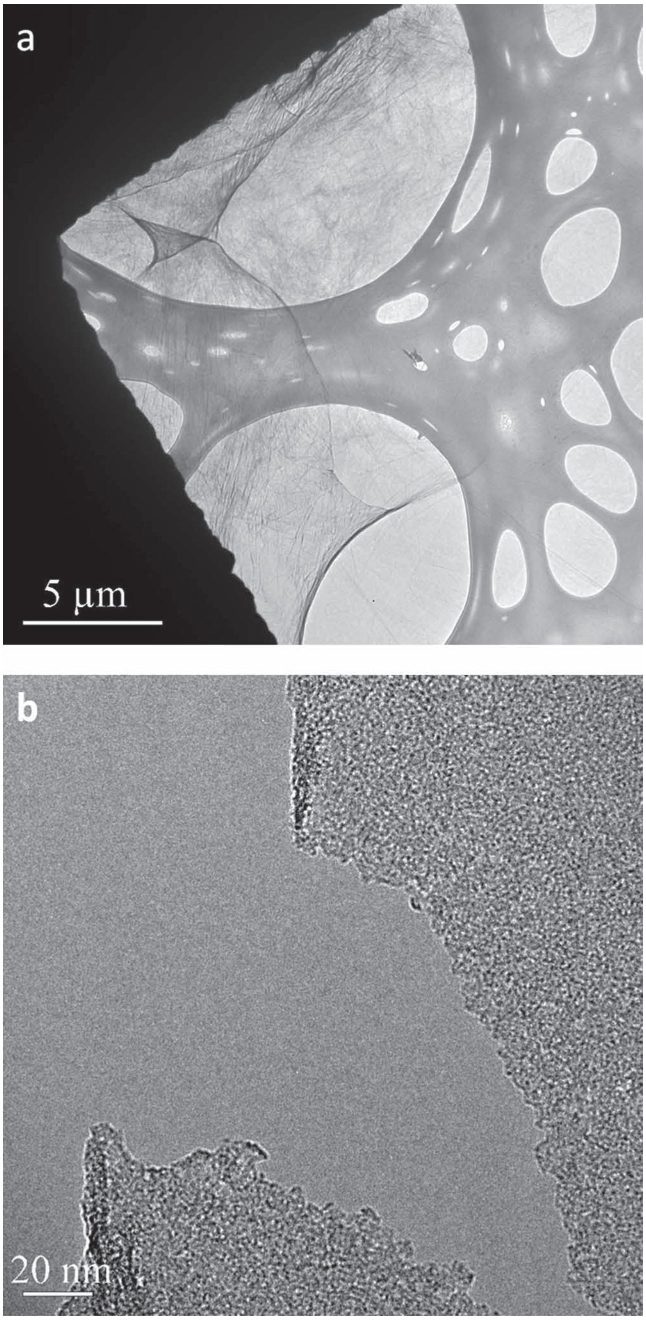

Figure 3. a) TEM micrograph of the GO sheets. b) TEM micrograph of a fractured GO sheet showing the monolayer nature.

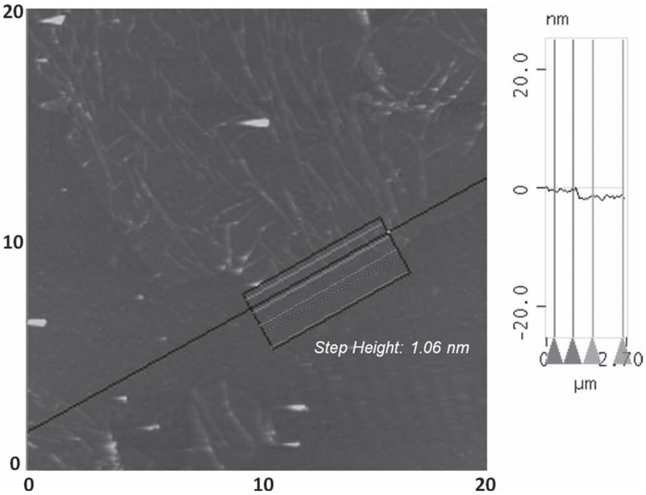

Figure 4. Tapping mode AFM image of a single-layer GO sheet and the corresponding height profile of the GO sheet.

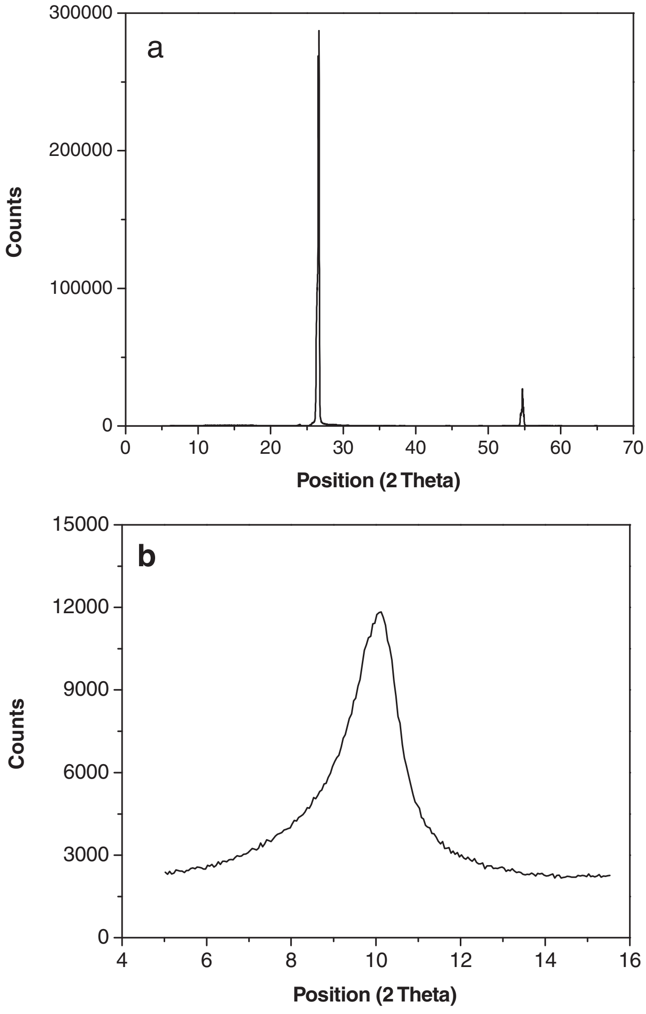

Figure 5. a) XRD pattern of natural graphite flakes. b) XRD pattern of an as-prepared GO sheet.

patterns of both the graphite flakes and the GO samples, indicating that the starting material represented a fully graphitic system with a sharp (002) peak, while the as-prepared GO had a distinct peak at $2\theta = 10.1°$, corresponding to a d-spacing of about 8.78 Å according to Bragg's law: $2d\sin\theta = n\lambda$, where n is an integer determined by the given order, and λ is the wavelength. This d-spacing value represents, approximately, a one-molecule-thick layer of water entrapped between the GO layers, presumably through a hydrogen bond. A recent theoretical study[13] also suggested that the water content controls the extent of these interlayer hydrogen-bond networks, thereby affecting the interlayer spacing. The individual GO platelets are interlinked via a non-uniform network of hydrogen bonds mediated by oxygenated functional groups and water molecules. This means that the interlayer spacing of GO sheets is proportional to the degree of oxidation. The mean crystallite size of the GO sheets that were oriented perpendicular to the diffracting plane in the dried suspension was calculated from the half-width-at-full-maximum (HWFM) value of the X-ray diffraction peak using Scherrer's equation, and was found to be 7.6 ± 0.3 nm.

The results from the X-ray-photoelectron-spectroscopy (XPS) analysis are shown in **Figure 6**. The C1s spectra are compared between the GO sheets obtained before and after reduction (rGO). The oxygen-to-carbon ratio decreased remarkably after the solution-phase reduction, implying an efficient removal of oxygen functional groups by decomposition of these groups and simultaneous restoration of the sp^2 C–C bonds.[36] The spectra were deconvoluted into four peaks corresponding to the following functional groups: carbon sp^2 (C=C), carbon sp^3, epoxy/hydroxyl (C–O), carbonyl (C=O) and carboxylate (O–C=O), and the summary is presented in **Table 1**. Judging from the deconvoluted curves, it can be said that the reduction process was successful in eliminating oxidized carbon in the form of carbonyl and epoxy/hydroxyl groups, simultaneously reducing the O/C ratio (**Figure 7**). The sp^2 hybridized C1s peak at 284.5 eV, with a well-defined symmetric shape, is attributed to pristine graphene.

The elemental compositions were analyzed based on the XPS spectra. The general spectra (Figure 6a and 6b) indicate that both the GO and rGO contained sulfur (0.4 and 0.17 wt%, respectively) and nitrogen (0.05 and 3.9 wt%, respectively), the latter of which is typical of hydrazine-reduced GO products. Hydrazine readily reacts with epoxide functional groups, resulting in the formation of hydrazine alcohols, which are mainly responsible for the detection of the large amount of nitrogen in rGO. Upon reduction, the oxygen content fell from 42 to 13.8 wt% while the O/C ratio decreased from 0.77 in GO to 0.16 in rGO, indicating the effectiveness of the hydrazine reduction. These observations are in good agreement with literature values for rGOs: the C content ranges from 60 to 86.4 wt%, the O content ranges from 11.3 to 34.6 wt%, whereas the N content ranges from 3.0 to 5.7 wt% after different reduction strategies.[37]

A major issue arising during Raman spectroscopy is damage to the samples induced by laser heating, because the GO and rGO samples could undergo local decomposition when irradiated with focused laser spots even at moderate power levels.[38] The Raman spectra shown in **Figure 8** indicate a marginal increase in the D to G band intensity ratio, I_D/I_G, from 0.85 to

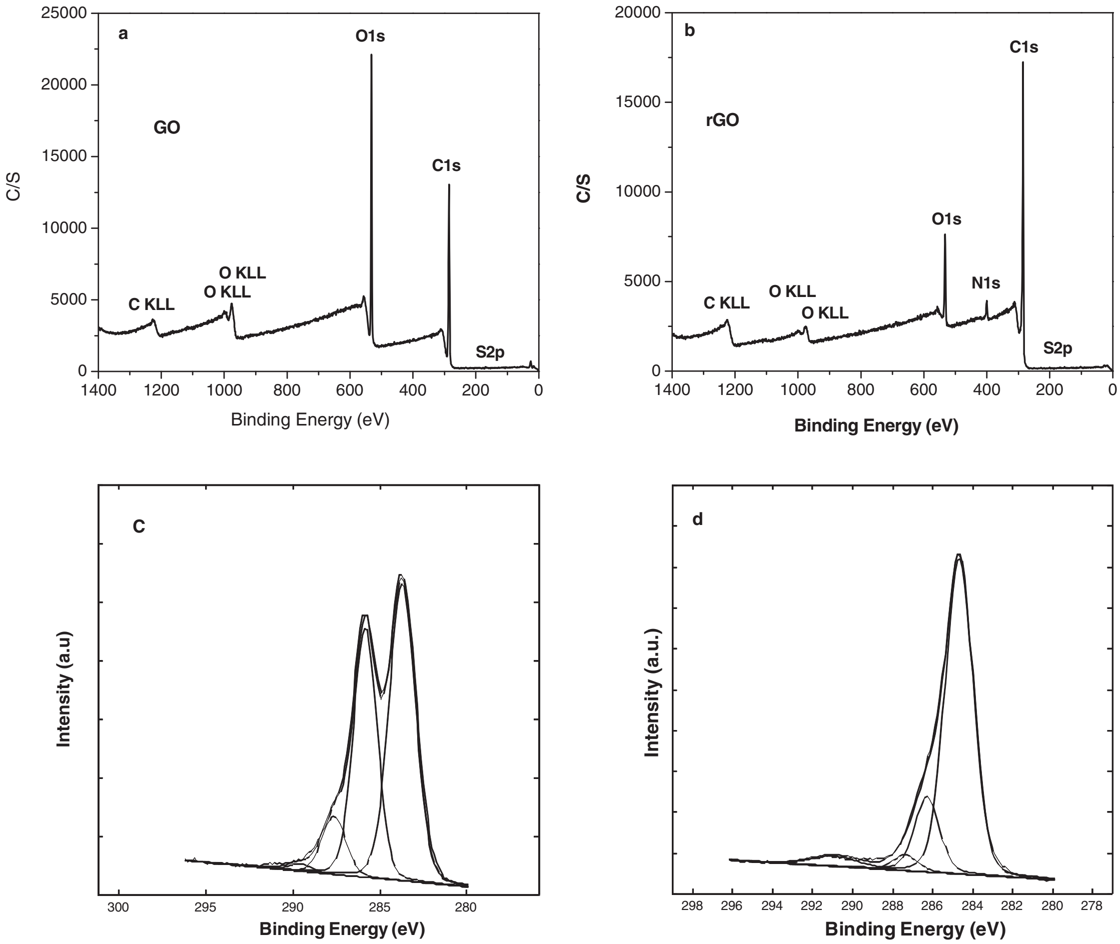

Figure 6. a) XPS general spectrum of GO. b) XPS general spectrum of rGO. c) Curve-fitted spectrum of GO. d) Curve-fitted spectrum of rGO.

0.89, as well as a marginal red shift of the G peak position upon reduction to rGO. Although a prominent D peak is a reflection of disorder in the carbon structure, the above observations are consistent with previous reports on similar rGO.[36–41] The stronger D peak intensity observed in rGO might be due to the smaller size of the graphene sheets and some remaining functionalities.[39] The increased edge area arising from the smaller graphene size after reduction corresponds to more defects. The decrease in the size of the newly formed graphene-like sp^2 domains is also partly responsible for the increase in the intensity ratio, I_D/I_G.[40] Ferrari et al.[41] also proposed that the GO is in an amorphous state and a graphite-like state is only recovered after reduction, implying that the intensity ratio cannot be directly compared between the two states.

Table 1. Summary of the relative percentages of the carbon and assignation.

Binding energy (eV) and assignation	284.5 eV C–C	286.0–286.7 eV C–O	287.6–287.8 eV –C=O	289.0–289.4 eV O–C=O
GO	48.6	36.8	9.5	5.2
rGO	75.5	16.7	3.5	4.3

Figure 9 illustrates the UV–vis spectra, indicating a red-shift of the absorption peak of the GO dispersion at a wavelength from 231 nm to 270 nm upon reduction by hydrazine.

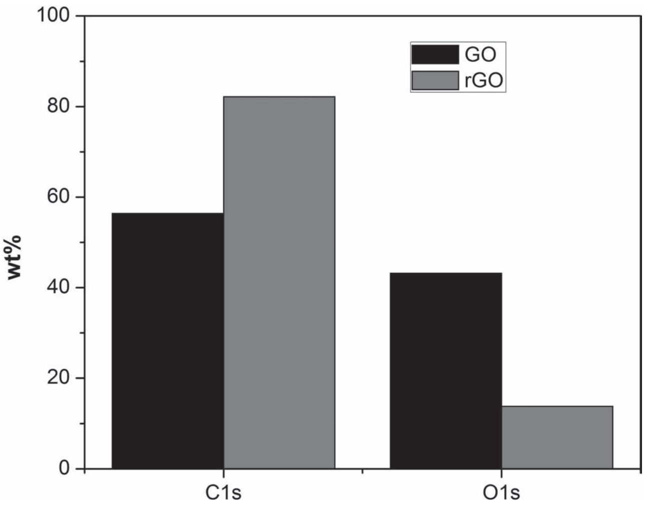

Figure 7. Changes in the weight percentages of carbon and oxygen in GO before and after reduction.

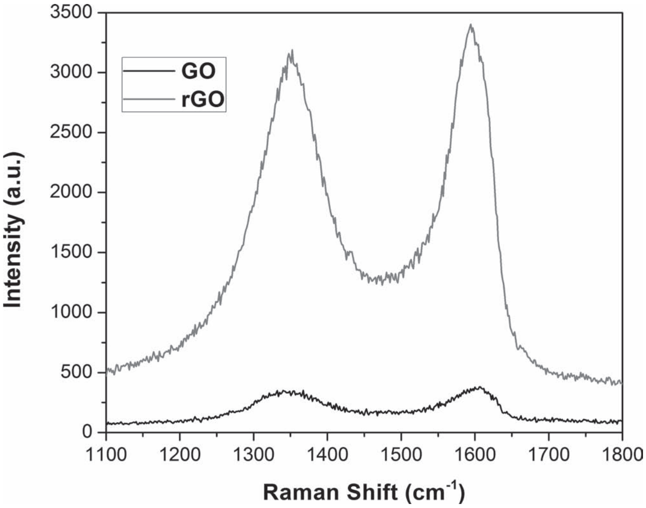

Figure 8. Raman spectra of GO and rGO.

The absorption in the whole spectral region increased after reduction. The peak in the region of 227–231 nm determines the degree of the remaining conjugation (π-π* transition).[35,42] The shoulder at around 300 nm can be ascribed to the n-π* transition of carbonyl groups. The large extinction coefficient observed here is indicative of aromatic rings or isolated aromatic domains being retained. The red-shift observed in rGO suggests that the electronic conjugation within the graphene sheets is restored upon reduction.[42]

2.2. Nematic Liquid Crystallinity of GO Suspensions

A series of aqueous dispersions with varying GO concentrations in deionized (DI) water were examined under a polarized optical microscope in transmission mode to evaluate their homogeneity and birefringence. Under crossed-polarizers, the system showed birefringence typical of liquid crystals, as shown in **Figure 10**. The spontaneous formation of lyotropic nematic liquid crystals was observed above a critical concentration of as low as ≈0.1 wt%. The critical GO concentration of 0.1 wt%, equivalent to ≈1.0 mg mL^{-1}, obtained here is, to the authors' knowledge, the lowest value among those reported for any liquid-crystalline colloids: see **Table 2** for comparison with reported crystalline liquids.

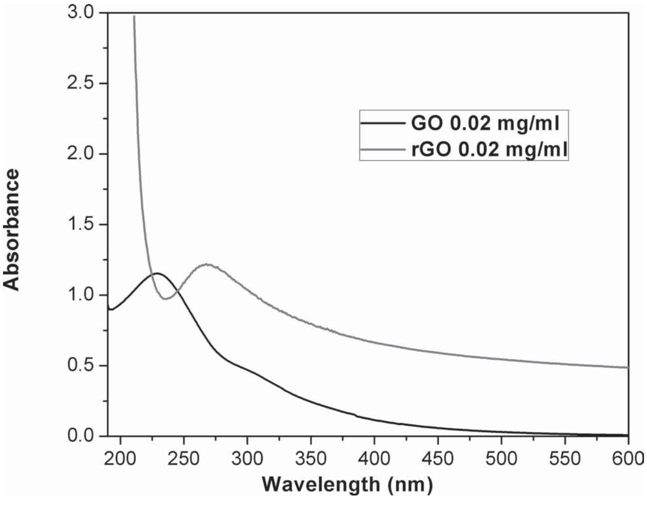

Figure 9. UV–vis spectra of as-prepared GO suspension and rGO.

Liquid crystallization occurred at such a low GO content owing to the ultrahigh aspect ratio, greater than ≈30 000, of the GO sheets (see Figure 2b). Similar to the other liquid-crystalline colloids,[29,44,45] steric hindrance arising from the overlapping of colloidal particles in concentrated dispersions results in an entropy-driven arrangement, forcing the particles to shape into a long-range order that resembles liquid-crystal molecules. The transition concentration depends largely on the size and shape of the particles, and is directly proportional to the density of the colloidal particles, ρ (in number of particles per unit area). Theoretical studies demonstrate that the transition happens when ρD^3 reaches a critical value of 4.12, where D is the disk diameter.[45] Assuming a disk shape of the GO sheets, their volume V_{GO} is given by:

$$V_{\mathrm{GO}} = \frac{\pi}{4} D^2 t \tag{1}$$

where t is the thickness of the GO sheets. For a GO dispersion with a concentration C (in g m^{-3}), ρ is calculated as follows:

$$\rho = \frac{C}{V_{\mathrm{GO}}\, d} \tag{2}$$

where d is the mass density of the GO sheets (in g cm^{-3}). Assuming d to be 2.2 g cm^{-3}, ρD^3 is obtained as:

$$\rho D^3 = \frac{C.D}{\frac{\pi}{4} t\, d} \tag{3}$$

The aspect ratio $\alpha = D/t$ and $d = 2.2 \times 10^6$ g m^{-3}; thus, ρD^3 is given by Equation 4:

$$\rho D^3 = \frac{C\alpha}{1.73 \times 10^6} \tag{4}$$

The units of the constant, 1.73×10^6, are g m^{-3}. Based on a Monte Carlo simulation for rigid platelets[46] and assuming that the colloid contains entirely monolayer GO sheets with an effective surface area of 2000 m^2 mL^{-1}, a transition concentration as low as 0.024 wt% or 240 g m^{-3} is expected, a few times lower than the 0.1 wt% shown in Figure 10.

The large discrepancy between the experiment and the prediction can be attributed to the flexible nature of the monolayer GO sheets and their polydispersity in size and thickness. The flexibility of the negatively charged GO sheets encourages interparticle interactions in aqueous media in the form of charge stabilization and double-layer extension.[46] The tendency of wrinkling of the GO sheets, especially in the presence of attached functional groups,[42] may be partly responsible for the higher experimental critical value observed in this study. Judging from the inverse relation between the transition concentration and the aspect ratio of the GO sheets, it can be seen that for GO sheets with a typical size in the range of few hundred nanometers to a few micrometers, a critical concentration on the order of 10–50 mg mL^{-1} is required to achieve liquid crystallinity. This value is approximately one order of magnitude higher

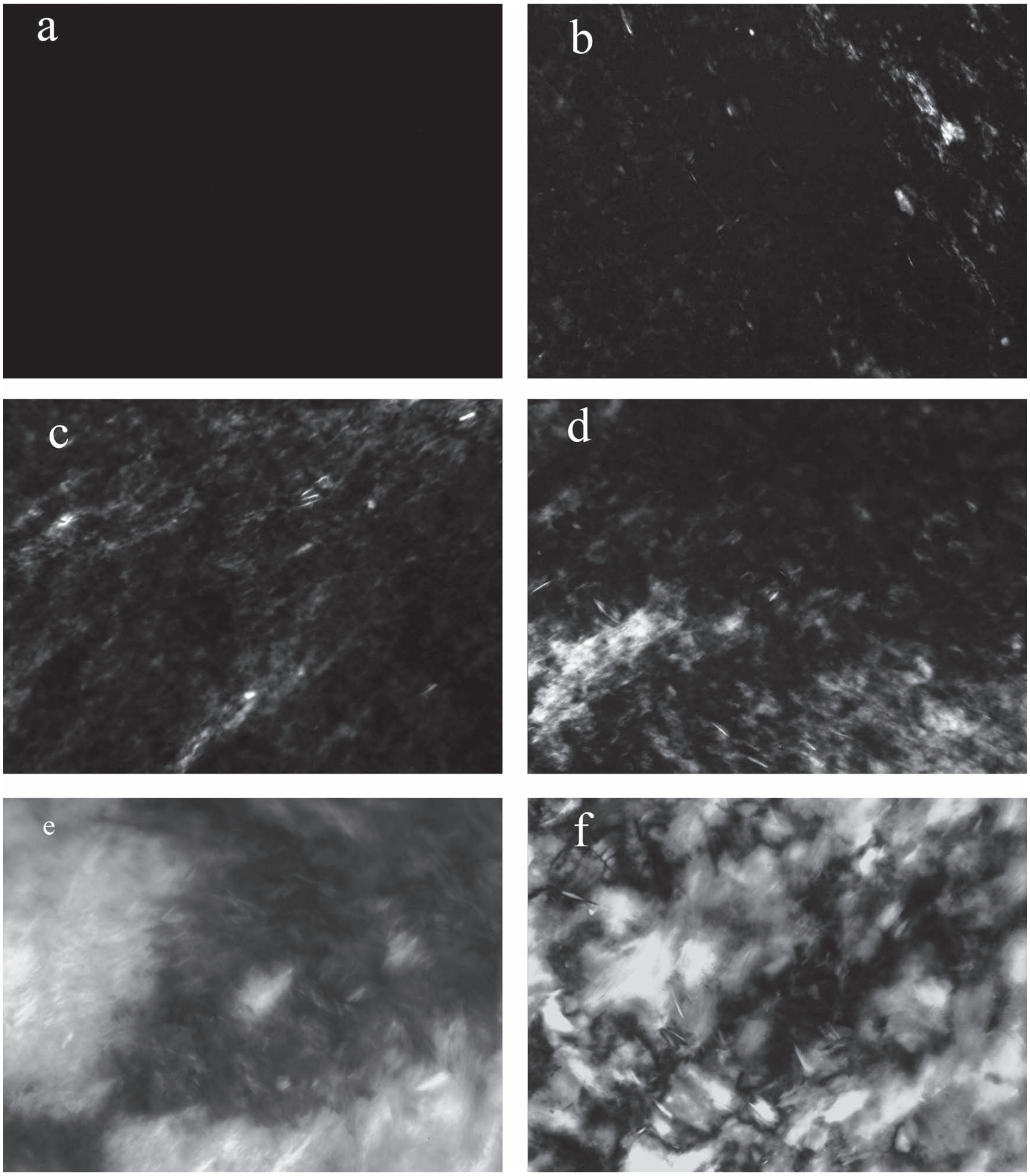

Figure 10. Aqueous dispersions of GO in DI water showing lyotropic nematic liquid crystals for GO contents above 0.1 wt%: a) 0.05 wt% GO; b) 0.1 wt% GO; c) 0.15 wt% GO; d) 0.2 wt% GO; e) 0.5 wt% GO; f) 1.0 wt% GO.

Table 2. Critical-concentration values reported for crystalline liquids.

Type of filler	Medium	Critical filler concentration
Modified polyisobutylene[22]	Toluene	950 mg mL^{-1}
Multiwalled CNTs[23]	Water	4.3 vol% (43–86 mg mL^{-1})
CNTs[43]	Water	5 wt% (24.94–49.88 mg mL^{-1})
Graphene[28]	Chlorosulphonic acid	20–30 mg mL^{-1}
Graphene oxide (current work)	Water	0.1 wt% (1 mg mL^{-1})

than the experimental concentration achieved in this study. A recent report[28] also demonstrated an isotropic-nematic transition in a graphene dispersion in superacid at a concentration of 20–30 mg mL^{-1}, which indicates the presence of graphene sheets with a low aspect ratio. Liquid crystals in suspensions containing rod-like particles suggest that polydispersity is one of the main reasons behind the shift of the biphasic region to a lower density and the broadening.[47] Even a change in the shape of the disks can have a large influence on attraction among the disks, a phenomenon that might play an important role here.

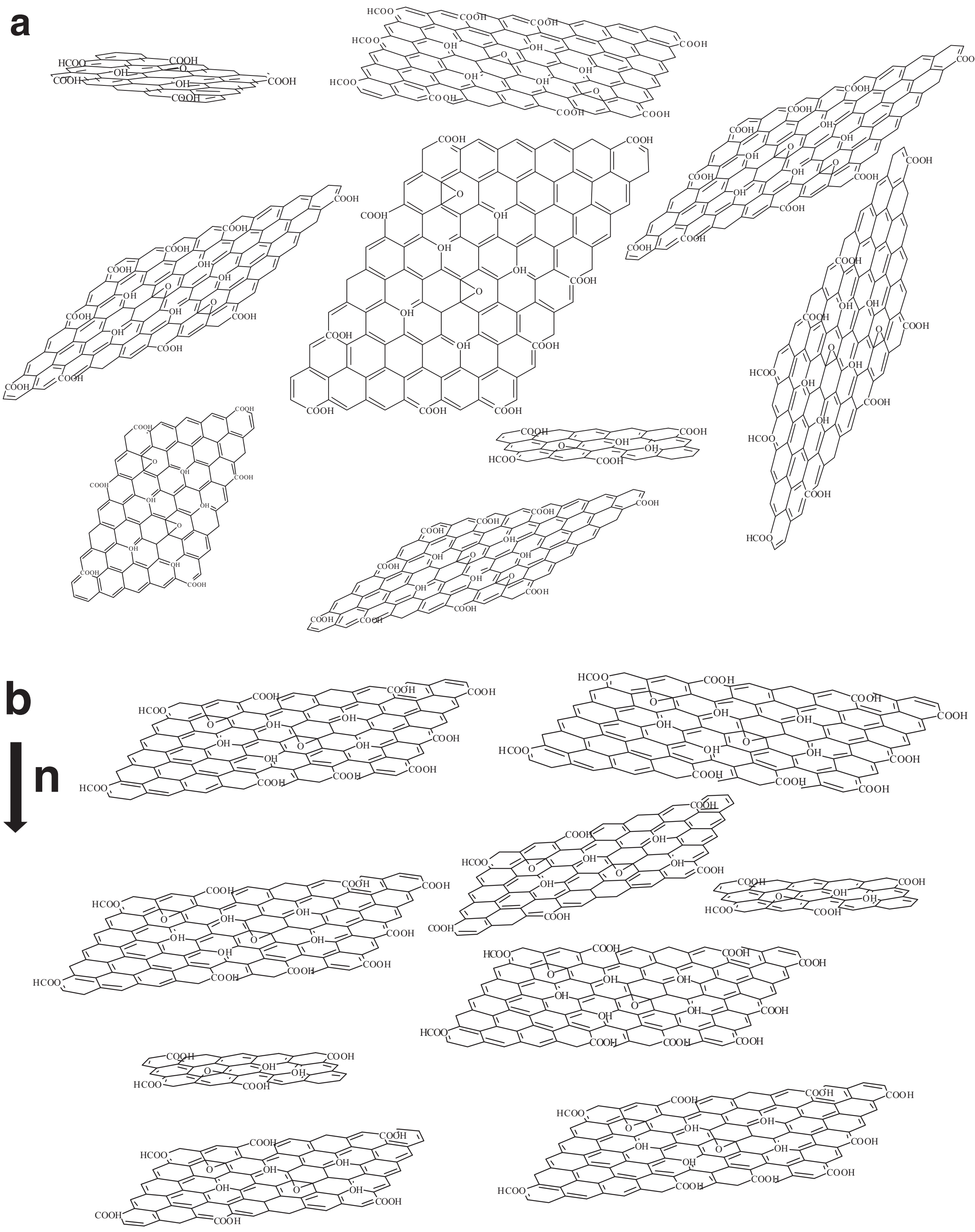

Figure 11. a) Isotropic phase of a GO aqueous dispersion showing a random distribution. b) Nematic phase of a GO aqueous dispersion showing alignment of the GO sheets with an orientation vector *n* perpendicular to the GO planes.

Apart from the high degree of anisotropy, self-assembly of the GO sheets into a liquid-crystalline phase is also affected by intermolecular interactions among them. The GO functionality is similar to that of 2D amphiphilic macromolecules; therefore, GO sheets exhibit a high affinity to minimizing the free energy of the system through intermolecular interactions of the hydrophobic parts (i.e., graphenic domains). It has been found that GO sheets with different sizes have face-to-face interactions with almost no repelling barrier, as the charged groups are mainly located at the edges.[32] The GO sheets obtained in this study were of high polydispersity in size, which in turn facilitated the face-to-face interactions by the stacking of the GO sheets into an aligned, layered structure and encouraged the formation of oriented liquid-crystalline domains. Therefore, in addition to the size of the GO sheets, other parameters such as the pH value and the electrolyte concentration can affect the liquid crystallinity of GO dispersions, as they can alter the intermolecular interactions.

The GO dispersion in an aqueous medium can readily form a nematic liquid-crystalline phase upon introduction of a high content of GO sheets. **Figure 11** schematically illustrates the transition from an isotropic to a nematic liquid-crystal phase. In contrast to the isotropic phase where the GO sheets show a random distribution, GO sheets with a high aspect ratio tend to align perpendicular to the GO planes with an orientation vector *n*. Although there are a number of different liquid-crystalline phases, such as nematic, chiral and columnar, reported for disk-shaped particles or the so-called discotics,[28] the only possible phase that can be formed in a system with polydisperse, unfunctionalized sheets is the nematic phase. In lyotropic phases, solvent molecules fill the space around the compounds to provide fluidity to the system. Therefore, the solvent should have a low viscosity to ensure the fluidity, facilitating easy accommodation and movement of the liquid-crystalline components. The formation of lyotropic liquid crystals depends on a delicate balance of the intermolecular interactions; thus, it is difficult to analyze the structure and properties of lyotropic liquid crystals. The fluidity in the nematic phases, although similar to the fluidity in isotropic liquids, can provide an easy path for alignment in the presence of an external force, indicating that the optical, electrical and mechanical properties of the liquid-crystal materials can be tailored by optimizing the external forces. Alignment and self-assembly of nanomaterials can be achieved in liquid-crystal phases. In contrast to CNT liquid crystals, GO can be aligned by applying a force in one direction. Alternatively, well-aligned GO structures can also be prepared by simple casting in an aqueous medium, as demonstrated below.

GO can be considered as an amphiphilic molecule[48] because it consists of different hydrophilic and hydrophobic parts. At a very-low concentration of GO with a high content of water, the GO dispersion can become totally random without any order. However, upon an increase in the concentration, the GO sheets fill up the space, forming a self-assembled structure. It is also proposed that, at high concentrations of GO, inverse phases might be observed where columns of water are encapsulated by the GO sheets. Functional groups attached onto the GO surface can also host polymer molecules. Furthermore, the high degree of anisotropy and high aspect ratio of GO sheets within the GO dispersion allow them to align in a specific direction. Such useful properties can also be exploited to fabricate self-aligned particle composites with a high degree of orientation when the particle content is above a critical value. To demonstrate the self-assembly and alignment of GO sheets, free-standing GO papers were fabricated by simple casting of GO dispersions and drying in ambient conditions, as shown in **Figure 12**. The self-assembled, free-standing GO paper exhibited a highly aligned, layered structure which was achieved without using sophisticated instruments or a vacuum-filtration technique. Various processes have been explored previously to make ordered assemblies using as-produced graphene or GO sheets, including dip-coating, vacuum-filtration[4,49] and Langmuir–Blodgett deposition.[32,50] However, in all of these techniques an external force is required to align the GO sheets. Based on the simple strategy that we propose in this study, composites with self-aligned GO sheets can be realized.[51]

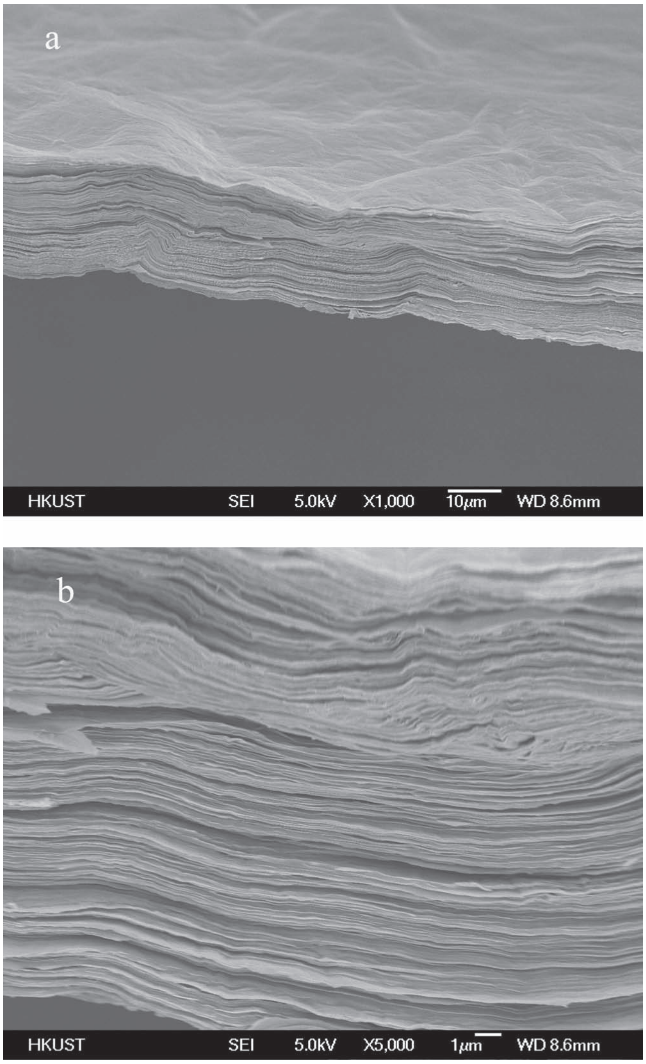

Figure 12. SEM micrographs of as-prepared GO paper at low (a) and high (b) magnification.

3. Conclusions

Stable dispersions of UL-GO were prepared employing a modified chemical method that involved pre-exfoliation of graphite. The use of exfoliated graphite instead of conventional graphite-intercalation compounds was aimed at minimizing possible breakage of the GO sheets during the chemical process. Upon the elimination of the sonication process, high yields of UL, monolayer GO sheets were obtained. The extremely high aspect ratio over 30 000 of the resultant GO sheets led to a liquid-crystalline transition in the aqueous colloidal suspension at a GO concentration as low as ≈1.0 mg mL^{-1} (0.1 wt%) through the self-alignment process. It is proposed that the ability to form self-assembled fillers at such a low GO concentration can be applied in many applications, including, for example, electrodes in energy-storage devices and a self-aligned brick-like GO structure in nanocomposites.

4. Experimental Section

Preparation of UL-GO: Natural graphite flakes (Asbury Graphite Mills, US) and sulfuric acid (H_2SO_4) (95.5–96.5%, General Chemical) were mixed and stirred in a round-bottom flask at a speed of 200 rpm. Fuming nitric acid (HNO_3) (Fisher) was then added into the mixture. The mixture was kept at room temperature and stirred for 24 h. Deionized water was then poured slowly into the mixture. The resulting mixture was washed using DI water three times, followed by centrifugation and drying at 60 °C for 24 h to obtain graphite-intercalation compounds (GICs). To obtain fully oxidized graphite and preserve the high initial lateral sizes of the graphite flakes, as well as to improve the yield of the process, expanded graphite (EG) was used to obtain the GO dispersions. The dry GIC powder was thermally expanded at 1050 °C for 15 s to obtain EG, whose thickness was typically in the range of ≈5–100 nm.

1 g of EG and 200 mL of sulfuric acid were mixed and stirred in a three-necked flask. 10 g of $KMnO_4$ was added to the mixture dropwise. The mixture was transferred into an ice bath, and 200 mL of deionized water and 50 mL of H_2O_2 were poured slowly into the mixture, realizing a colour change of the suspension to light brown. Having stirred for another 30 min, the GO particles were then washed and centrifuged with a HCl solution (9:1 water:HCl by volume), then centrifuged again and washed with deionized water until the pH of the solution became about 5 to 6. The GO particles were then diluted using DI water and exfoliated by gentle shaking. The individual GO sheets thereby obtained were reduced to graphene sheets by adding a hydrazine solution (the ratio of hydrazine to GO being about 3:1) to the dispersion, which was then heated at 80 °C for 24 h. To evaluate the liquid crystallinity of the samples, the GO dispersions in DI water were prepared with different concentrations, up to 10 mg mL^{-1}, equivalent to 1 wt% of GO. To prepare the GO films, a 5 mg mL^{-1} GO dispersion was homogenized by gentle shaking. The dispersion was stabilized for a few days until all of the air bubbles were removed, and was then cast on a cellulose ester filter membrane and dried at 50 °C for 24 h. Finally, the membrane was dissolved in acetone and the GO film was extracted. The free-standing, flexible GO paper was examined using SEM (JSM 6700F, JEOL) at a 2 kV accelerating voltage to evaluate the alignment of the GO sheets.

Characterization: To visualize the GO sheets under an optical microscope (OM), 130–140 nm thick layers of SiO_2 on the surface of the Si wafers were fabricated, based on the Deal Groove oxide-growth-kinetics model, which is only valid for the temperature range of 700–1300 °C and oxide thicknesses up to 2 µm. 3-Aminopropyltriethoxysilane (APTES) (Aldrich*)* was mixed with water and one drop of hydrochloric acid (Sigma–Aldrich) was added to the solution. The as-prepared Si substrates were then introduced into the aqueous silane solution for 30 min to silanize them and washed thoroughly with DI water. The substrate was then dipped in the GO solution for 10 s and was subsequently introduced into the DI water and dried. The GO sheets were examined under an optical microscope (Olympus BH2-DMA). Aqueous dispersions with different concentrations of GO in DI water were examined under the polarized optical microscope in transmission mode to evaluate the homogeneity and birefringence of the GO sheets.

In the SEM, secondary-electron (SE) signals can be used to obtain high quality images, but a major issue in employing SEs is the inherently high sensitivity to surface charging. Therefore, it is hard to produce SEM images with SE with insulating samples like GO sheets.[31,32] The morphology of the GO samples was examined by SEM without gold coating. Thus, the insulating GO sheets deposited on the SiO_2 coating/Si substrate prepared for optical microscopy were directly examined by SEM. The image was acquired using an SE detector, which allowed high-throughput examination of the GO sheets over millimeter-scale areas. However, because the GO layer was deposited on the insulating SiO_2/Si substrate and no Au coating was applied, it was inevitable to find some burnt spots and unwanted carbonaceous contamination, especially when high acceleration voltages or short working distances were used.

The GO samples were also examined by TEM (JEOL 2010F FEG TEM). The TEM samples were prepared by drying a droplet of the GO suspension on a holey carbon grid. Tapping-mode AFM (Digital Instruments Multimode AFM, Nanoscope) was used to acquire the images of the GO under ambient conditions. The samples prepared for the above SEM examination were also used for the AFM observations. The XRD studies were performed using a powder XRD system (Philips1825) with Cu Kα radiation (λ = 0.154 nm), operating at 40 keV and with a cathode current of 20 mA, to characterize the interlayer spacing of the GO samples. To prepare the samples, droplets of the suspensions were dried in air on a cellulose acetate filter. The GO and reduced-GO samples were evaluated by UV–vis spectroscopy (Perkin–Elmer Lambda 20). Raman spectroscopy (Renishaw MicroRaman/Photoluminescence System) was used to analyze the samples using a 514 nm He-Ne laser. The elemental composition was characterized by XPS (PHI5600 Physical Electronics) with a pass energy of 26.00 eV, a 45° takeoff angle and a beam size of 100 µm.

Acknowledgements

This project was supported by the Research Grant Council of Hong Kong SAR (Project No. 614010). Q.B.Z was partly supported by the Nanotechnology Program of the School of Engineering at HKUST. Technical assistance from the Materials Characterization and Preparation Facilities (MCPF) of HKUST is appreciated.

Received: February 27, 2011
Revised: April 10, 2011
Published online: June 3, 2011

---

[1] D. R. Dreyer, S. Park, C. W. Bielawski, R. S. Ruoff, *Chem. Soc. Rev.* **2010**, *39*, 228.
[2] K. S. Novoselov, A. K. Geim, S. V. Morozov, D. Jiang, Y. Zhang, S. V. Dubonos, I. V. Grigorieva, A. A. Firsov, *Science* **2004**, *306*, 666.
[3] X. Zhou, Z. Liu, *Chem. Commun.* **2010**, 2611.
[4] D. A. Dikin, S. Stankovich, E. J. Zimney, R. D. Piner, G. H. B. Dommett, G. Evmenenko, S. T. Nguyen, R. S. Ruoff, *Nature* **2007**, *448*, 457.
[5] C. Petit, M. Seredych, T. J. Bandosz, *J. Mater. Chem.* **2009**, *19*, 9176.
[6] S. Park, R. S. Ruoff, *Nature Nanotechnol.* **2009**, *4*, 217.
[7] K. A. Mkhoyan, A. W. Contryman, J. Silcox, D. A. Stewart, G. Eda, C. Mattevi, S. Miller, M. Chhowalla, *Nano Lett.* **2009**, *9*, 1058.
[8] K. S. Kim, Y. Zhao, H. Jang, S. Y. Lee, J. M. Kim, K. S. Kim, J.-H. Ahn, P. Kim, J.-Y. Choi, B. H. Hong, *Nature* **2009**, *457*, 706.
[9] C. Berger, Z. Song, X. Li, X. Wu, N. Brown, C. Naud, D. Mayou, T. Li, J. Hass, A. N. Marchenkov, E. H. Conrad, P. N. First, W. A. de Heer, *Science* **2006**, *312*, 1191.
[10] B. C. Brodie, *Philos. Trans. R. Soc. London* **1859**, *149*, 249.
[11] W. S. Hummers, R. E. Offeman, *J. Am. Chem. Soc.* **1958**, *80*, 1339.
[12] L. Staudenmaier, *Ber. Dtsch. Chem. Ges.* **1898**, *31*, 1481.
[13] N. V. Medhekar, A. Ramasubramaniam, R. S. Ruoff, V. B. Shenoy, *ACS Nano* **2010**, *4*, 2300.
[14] C. Hontoria-Lucas, A. J. López-Peinado, J. d. D. López-González, M. L. Rojas-Cervantes, R. M. Martín-Aranda, *Carbon* **1995**, *33*, 1585.
[15] Y. Geng, S. J. Wang, J. K. Kim, *J. Colloid Interface Sci.* **2009**, *336*, 592.
[16] M. M. Gudarzi, F. Sharif, *J Colloid Interface Sci.* **2010**, *349*, 63.
[17] G. Eda, M. Chhowalla, *Nano Lett.* **2009**, *9*, 814.

[18] S. Wang, P. K. Ang, Z. Wang, A. L. L. Tang, J. T. L. Thong, K. P. Loh, *Nano Lett.* **2009**, *10*, 92.
[19] J. T. Robinson, F. K. Perkins, E. S. Snow, Z. Wei, P. E. Sheehan, *Nano Lett.* **2008**, *8*, 3137.
[20] X. Dong, C.-Y. Su, W. Zhang, J. Zhao, Q. Ling, W. Huang, P. Chen, L.-J. Li, *Phys. Chem. Chem. Phys.* **2010**, *12*, 2164.
[21] C. Valles, C. Drummond, H. Saadaoui, C. A. Furtado, M. He, O. Roubeau, L. Ortolani, M. Monthioux, A. Pénicaud, *J. Am. Chem. Soc.* **2008**, *130*, 15802.
[22] F. M. Van Der Kooij, K. Kassapidou, H. N. W. Lekkerkerker, *Nature* **2000**, *406*, 868.
[23] W. Song, I. A. Kinloch, A. H. Windle, *Science* **2003**, *302*, 1363.
[24] S. Zhang, I. A. Kinloch, A. H. Windle, *Nano Lett.* **2006**, *6*, 568.
[25] L. M. Ericson, H. Fan, H. Peng, V. A. Davis, W. Zhou, J. Sulpizio, Y. Wang, R. Booker, J. Vavro, C. Guthy, A. N. G. Parra-Vasquez, M. J. Kim, S. Ramesh, R. K. Saini, C. Kittrell, G. Lavin, H. Schmidt, W. W. Adams, W. E. Billups, M. Pasquali, W.-F. Hwang, R. H. Hauge, J. E. Fischer, R. E. Smalley, *Science* **2004**, *305*, 1447.
[26] S. E. Moulton, M. Maugey, P. Poulin, G. G. Wallace, *J. Am. Chem. Soc.* **2007**, *129*, 9452.
[27] M. Bravo-Sanchez, T. J. Simmons, M. A. Vidal, *Carbon* **2010**, *48*, 3531.
[28] N. Behabtu, J. R. Lomeda, M. J. Green, A. L. Higginbotham, A. Sinitskii, D. V. Kosynkin, D. Tsentalovich, A. N. G. Parra-Vasquez, J. Schmidt, E. Kesselman, Y. Cohen, Y. Talmon, J. M. Tour, M. Pasquali, *Nature Nanotechnol.* **2010**, *5*, 406.
[29] D. Frenkel, *Liq. Cryst.* **1989**, *5*, 929.
[30] R. Wang, J. Sun and L. Gao, *J. Phys. Chem. C* **2010**, *114*, 4923.
[31] J. Kim, F. Kim, J. Huang, *Mater. Today* **2010**, *13*, 28.
[32] L. J. Cote, F. Kim, J. Huang, *J. Am. Chem. Soc.* **2008**, *131*, 1043.
[33] R. R. Nair, P. Blake, A. N. Grigorenko, K. S. Novoselov, T. J. Booth, T. Stauber, N. M. R. Peres, A. K. Geim, *Science* **2008**, *320*, 1308.
[34] Q. B. Zheng, Y. Geng, S. J. Wang, Z. G. Li, J. K. Kim, *Carbon* **2010**, *48*, 4315.
[35] H. C. Schniepp, J.-L. Li, M. J. McAllister, H. Sai, M. Herrera-Alonso, D. H. Adamson, R. K. Prud'homme, R. Car, D. A. Saville, I. A. Aksay, *J. Phys. Chem. B* **2006**, *110*, 8535.
[36] C. Gómez-Navarro, J. C. Meyer, R. S. Sundaram, A. Chuvilin, S. Kurasch, M. Burghard, K. Kern, U. Kaiser, *Nano Lett.* **2010**, *10*, 1144.
[37] W. Gao, L. Alemany, L. Ci, P. Ajayan, *Nature Chem.* **2009**, *1*, 403.
[38] B. Krauss, T. Lohmann, D. H. Chae, M. Haluska, K. von Klitzing, J. H. Smet, *Phys. Rev. B: Condens. Matter* **2009**, *79*, 165428.
[39] W. Gao, L. B. Alemany, L. Ci, P. M. Ajayan, *Nature Chem.* **2009**, *1*, 403.
[40] D. Yang, A. Velamakanni, G. Bozoklu, S. Park, M. Stoller, R. D. Piner, S. Stankovich, I. Jung, D. A. Field, C. A. Ventrice Jr, R. S. Ruoff, *Carbon* **2009**, *47*, 145.
[41] A. C. Ferrari, J. Robertson, *Phys. Rev. B: Condens. Matter* **2000**, *61*, 14095.
[42] D. C. Marcano, D. V. Kosynkin, J. M. Berlin, A. Sinitskii, Z. Sun, A. Slesarev, L. B. Alemany, W. Lu, J. M. Tour, *ACS Nano* **2010**, *4*, 4806.
[43] N. Puech, C. Blanc, E. Grelet, C. Zamora-Ledezma, M. Maugey, C. c. Zakri, E. Anglaret, P. Poulin, *J. Phys. Chem. C* **2011**, *115*, 3272.
[44] D. Frenkel, *J. Phys. Chem.* **1987**, *91*, 4912.
[45] R. Eppenga, D. Frenkel, *Mol. Phys.* **1984**, *52*, 1303.
[46] F. M. Van Der Kooij, H. N. W. Lekkerkerker, *J. Phys. Chem. B* **1998**, *102*, 7829.
[47] G. J. Vroege, H. N. W. Lekkerkerker, *J. Phys. Chem.* **1993**, *97*, 3601.
[48] J. Kim, L. J. Cote, F. Kim, W. Yuan, K. R. Shull, J. Huang, *J. Am. Chem. Soc.* **2010**, *132*, 8180.
[49] S. J. Wang, Y. Geng, Q. Zheng, J.K. Kim, *Carbon* **2010**, *48*, 1815.
[50] T. Szabó, V. Hornok, R. A. Schoonheydt, I. Dékány, *Carbon* **2010**, *48*, 1676.
[51] M. M. Gudarzi, S. H. Aboutalebi, N. Yousefi, Q. B. Zheng, F. Sharif, J. K. Kim, **2011**, unpublished.